Eur. Phys. J. A (2026) 62:46
https://doi.org/10.1140/epja/s10050-026-01823-6

THE EUROPEAN PHYSICAL JOURNAL A

Regular Article - Experimental Physics

Experimental and theoretical investigation of the ^{13}C+^{119}Sn reaction dynamics

L. M. Martinis[1], L. R. Gasques[1,a], V. Scarduelli[1], L. C. Chamon[1], W. A. Y. Hatano[1], J. K. L. Chaves[1], G. P. Cessel[1], E. S. Rossi. Jr.[1], L. Garrido-Gómez[2], J. P. Fernández-García[2], M. A. G. Alvarez[2]

[1] Universidade de Sao Paulo, Instituto de Fisica, Rua do Matao, 1371, Sao Paulo, SP 05508-090, Brazil
[2] Departamento FAMN, Universidad de Sevilla, Apartado 1065, 41080 Seville, Spain

Received: 11 November 2025 / Accepted: 21 February 2026

Communicated by Alessia Di Pietro

Abstract We report on the measurement and analysis of elastic scattering angular distributions for the ^{13}C+^{119}Sn system at two bombarding energies: 40.0 and 46.9 MeV. In addition, inelastic scattering and single-neutron transfer reactions were measured at 46.9 MeV. The data were obtained using the same experimental setup previously employed in the ^{12}C+^{119}Sn study, allowing for a direct comparison. Optical model analyses were performed using the São Paulo potential for the real part of the interaction, while the imaginary part was treated both phenomenologically and via normalization of the real potential. Coupled-reaction-channels calculations were carried out, including couplings to inelastic excitations and one-neutron transfer channels. This approach yielded an improved description of the elastic scattering data across the full angular range for both energies. A direct comparison with the ^{12}C+^{119}Sn results indicates that the additional neutron in ^{13}C enhances absorption from the elastic channel. These findings highlight the sensitivity of near-barrier reaction dynamics to moderately bound valence nucleons and underscore the importance of coupling effects in accurately describing heavy-ion interactions.

1 Introduction

Heavy-ion induced reactions at energies near the Coulomb barrier offer valuable insights into the interplay between nuclear structure and reaction dynamics. In particular, elastic and inelastic scattering, transfer, and fusion processes are known to be strongly affected by couplings to collective and single-particle excitations of the interacting nuclei. These couplings can lead to significant modifications of reaction observables relative to single-channel predictions, as successfully described within the framework of coupled-reaction-channels (CRC) calculations.

Previous studies involving carbon isotopes incident on light- and medium-mass targets have demonstrated the sensitivity of reaction mechanisms to both projectile structure and the nature of the coupling scheme [1–8]. In particular, the ^{12}C+^{119}Sn system was recently investigated [9], where a comprehensive set of experimental data, including elastic scattering and peripheral reaction cross sections, was analyzed using CRC calculations incorporating inelastic and transfer couplings. That study emphasized the importance of couplings to low-lying collective states in both projectile and target in reproducing the observed cross sections.

In the present work, we extend this investigation to the ^{13}C+^{119}Sn system (V_B = 42.5 MeV). To avoid ambiguity in terminology, we refer to ^{13}C as a moderately bound nucleus: its neutron separation energy is $S_n = 4.95$ MeV, larger than the characteristic thresholds of canonical weakly bound projectiles (e.g., ^{6}Li, ^{6}He) but smaller than the average binding per nucleon in heavy nuclei (≈ 8 MeV). The addition of one neutron to the ^{12}C core introduces new reaction channels and coupling schemes, particularly those involving one-neutron transfer and the possible influence of the valence neutron in ^{13}C. These features make the system an ideal case for exploring the impact of moderately bound nucleons on near-barrier reaction dynamics. As in the case of the ^{12}C+^{119}Sn reaction, we present angular distribution measurements performed at $E_{\rm Lab} = 46.9$ MeV. In addition to elastic scattering yields, significant contributions from inelastic excitations and both one-neutron pickup and stripping channels were observed. A complementary elastic scattering angular distribution was also measured at $E_{\rm Lab} = 40.0$ MeV.

The data were analyzed using two complementary formalisms. First, an optical model (OM) analysis was employed to describe the elastic scattering data. Subsequently, the CRC

[a] e-mail: lgasques@if.usp.br (corresponding author)

Published online: 09 March 2026

approach was used to incorporate the relevant couplings and extract information about the underlying reaction mechanisms. In all calculations, the parameter-free São Paulo potential (SPP) [10,11] was adopted as the bare interaction.

This paper is organized as follows. The experimental setup and data analysis are described in Sect. 2. The experimental results and CRC calculations are presented in Sect. 3. A summary and the main conclusions are given in Sect. 4.

2 Experimental setup and data analysis

The experiment was performed at the 30B beamline of the Open Laboratory of Nuclear Physics and Applications (LAFNA, in Portuguese) at the Institute of Physics, University of São Paulo. A ^{13}C beam was accelerated using an 8 MV tandem accelerator and directed onto a ^{119}Sn target with a thickness of approximately 130 μg/cm^2. A thin layer of ^{197}Au ($\sim 40\ \mu$g/cm^2) was evaporated over the ^{119}Sn to allow for normalization of the measured cross sections. At the energies and angles of the present experiment, the elastic scattering cross section on the gold layer is purely Rutherford and therefore provides an absolute normalization of the experimental cross sections. An average energy loss of approximately 100 keV for the ^{13}C incident beam at the center of the composite target has been accounted for in the analysis.

For both bombarding energies, at sufficiently forward angles, the elastic scattering cross sections for the ^{13}C scattered onto the ^{119}Sn and ^{197}Au targets are dominated by the Coulomb interaction and can therefore be described by the classical Rutherford formula. By assuming that the ratio of the measured differential elastic scattering cross section to the Rutherford prediction equals unity in this angular region, a normalization factor can be extracted and applied to scale the cross sections over the full angular range.

The same setup previously described in detail in Ref. [9] was employed in the present experiment. For a comprehensive description of the setup, we refer the reader to that earlier publication. The overall experimental arrangement, including target specifications, detector geometry, and data acquisition system, remained unchanged. Charged particles produced during the ^{13}C+^{119}Sn reaction were collected by the STAR (Silicon Telescopes Array for Reactions) device, consisting of a combination of two segmented large-area detectors (50 mm $\times$ 50 mm). A third thick PAD detector was mounted in the back of the telescope, forming a triple-telescope configuration.

Particle identification was performed based on energy loss measurements of ΔE and residual energy E_R. After calibrating the energy response of each strip in both ΔE and E detectors, the experimental energy loss (ΔE_{exp}) of incident ^{13}C ions was determined for each pixel. However, thin large-area silicon detectors exhibit significant thickness non-uniformity across their active area (e.g., [12]), resulting in a substantial spread in the energy loss of charged particles striking individual pixels. Since the energy loss of punch-through ions depends on the detector thickness, it is useful to define the so-called reduced energy loss as the ratio between the experimental and theoretical energy losses: $\Delta E_{red} = \Delta E_{exp}/\Delta E_{theo}$. In this work, theoretical energy loss values (ΔE_{theo}) were calculated using the STOPX code [13]. The reduced energy loss is independent of detector thickness and allows for reliable summation of events across different pixels.

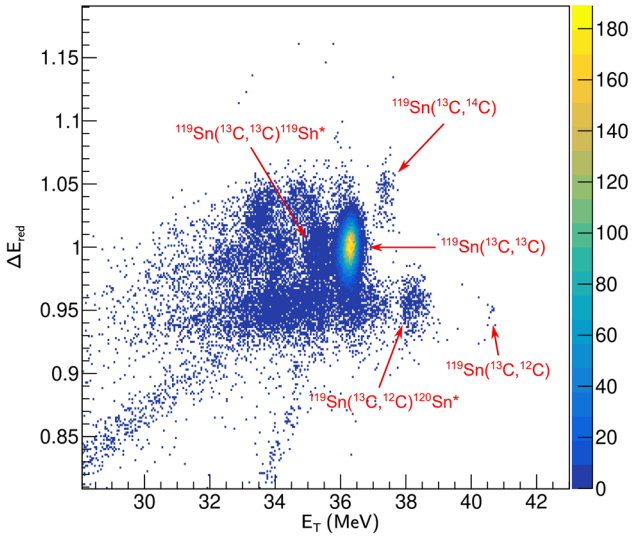

Fig. 1 Two-dimensional (ΔE_{red}, E_T) spectrum measured at $E_{\text{Lab}} =$ 46.9 MeV for the ^{13}C+^{119}Sn reaction. The data correspond to a detector pixel located at $\theta_{\text{Lab}} = 100°$. Peaks associated with elastic and inelastic scattering, as well as neutron transfer channels, are indicated

A two-dimensional (ΔE_{red}, E_T) spectrum is shown in Fig. 1, where $E_T = \Delta E + E_R$. Distinct yields corresponding to the elastic and inelastic scattering of ^{13}C are observed, as well as events associated with the detection of ^{12}C and ^{14}C, which are attributed to neutron stripping and pickup transfer processes, respectively.

In the present work ^{119}Sn was chosen as the target because, through single-neutron transfer, both the residual nucleus and the ^{13}C projectile transform into even–even systems. These nuclei have well-separated low-lying excited states, which results in a better energy resolution of the yields observed in the spectra.

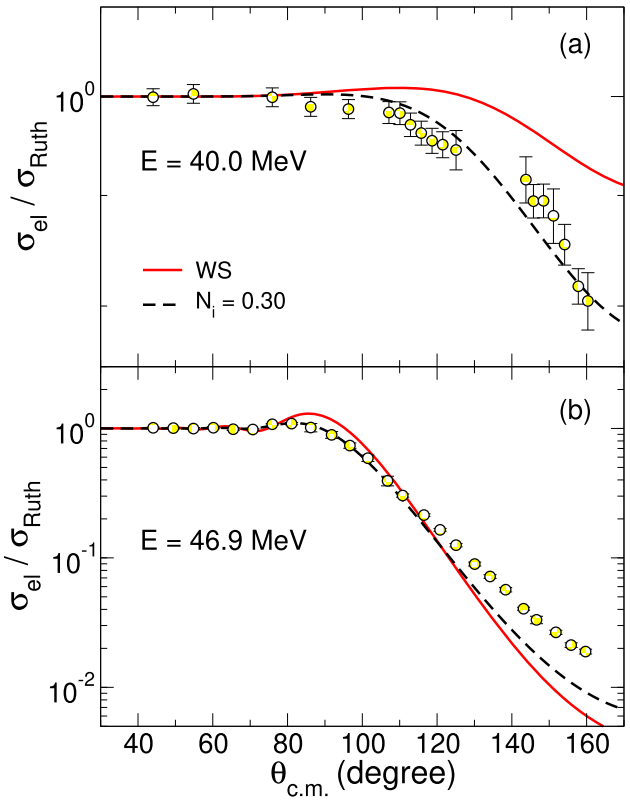

Fig. 2 Elastic scattering cross sections for the ^{13}C+^{119}Sn system measured at 40.0 MeV (**a**) and 46.9 MeV (**b**). The solid red and dashed black lines represent OM calculations using, respectively, an internal WS imaginary potential and an imaginary potential defined as $W(R) = 0.30\, V_{\rm SPP}(R)$

3 Experimental and theoretical results

In this work, we report new measurements of the elastic scattering angular distributions for the ^{13}C+^{119}Sn system at $E_{\rm Lab} = 40.0$ and 46.9 MeV. The yields corresponding to the $3/2^+$ excited state of ^{119}Sn at 23 keV could not be experimentally separated from those of the elastic channel. However, CRC calculations performed at both bombarding energies indicate that the contribution from this inelastic transition is negligible compared to the elastic scattering cross section and does not significantly affect the extracted data.

We have also investigated the effect of including the spin–orbit potential for both the projectile and the target in the calculations. At the bombarding energies considered in the present work, the inclusion of these terms leads to no significant change in the elastic scattering angular distributions.

3.1 Optical model analysis

Panels (a) and (b) of Fig. 2 show the experimental data measured at 40.0 and 46.9 MeV, respectively, along with the results of an OM analysis performed using the SPP for the real part of the nuclear interaction. Two distinct approaches were considered for the imaginary part of the optical potential. The first employs a phenomenological Woods-Saxon (WS) form with parameters $W_0 = 80$ MeV, $r_{i0} = 0.8$ fm, and $a_i = 0.30$ fm. This choice yields an absorptive potential that is negligible near the nuclear surface, effectively accounting for flux loss through barrier penetration, typically associated with fusion. In contrast, the second approach models the imaginary potential by scaling the real part with a normalization factor N_i, thereby introducing significant surface absorption, which may be attributed to peripheral processes such as direct or transfer reactions.

As shown in Fig. 2, the solid red line, representing the OM calculation with the internal WS imaginary potential, provides a poor description of the elastic scattering data at both energies. In contrast, the dashed black line corresponds to a calculation in which the imaginary potential is defined as $W(R) = N_i\, V_{\rm SPP}(R)$, with $N_i = 0.30$ adjusted to optimize agreement with the data at both incident energies. This approach yields a notably improved fit over the entire angular range at the lower energy. At 46.9 MeV, the agreement is particularly enhanced in the Coulomb-nuclear interference region near $\theta_{\rm c.m.} = 80°$. Although this OM prescription, featuring only a single free parameter, significantly improves the description of the data, it still fails to reproduce the cross sections at backward angles.

3.2 Coupled-reaction-channel analysis

In addition to elastic scattering, significant contributions from inelastic excitations and both one-neutron pickup and one-neutron stripping channels were observed in the spectra for the experiment conducted at $E_{\rm Lab} = 46.9$ MeV. Accordingly, CRC calculations were performed using the SPP for the real part of the nuclear interaction [10,11]. As a first step, the same internal WS imaginary potential was adopted, with parameters $W_0 = 80$ MeV, $r_{i0} = 0.8$ fm, and $a_i = 0.30$ fm. Following the procedure adopted in the OM analyses, the strength of the imaginary potential was subsequently varied by adjusting the normalization factor N_i in order to obtain a satisfactory description of the data. The coupling scheme is represented in Fig. 3. The FRESCO code [14] was used for all calculations.

The inelastic couplings included in the CRC model are summarized in Table 1, which lists the spin, transition multipolarity, excitation energy, Coulomb transition probability, and deformation length for both projectile and target excited states. To determine the nuclear deformation parameters δ_λ from the Coulomb transition strengths, corrections due to the finite diffuseness of the nuclear density profile were taken into account [15,16]. Only the inelastic states with the largest coupling strengths are included in the CRC, since weaker

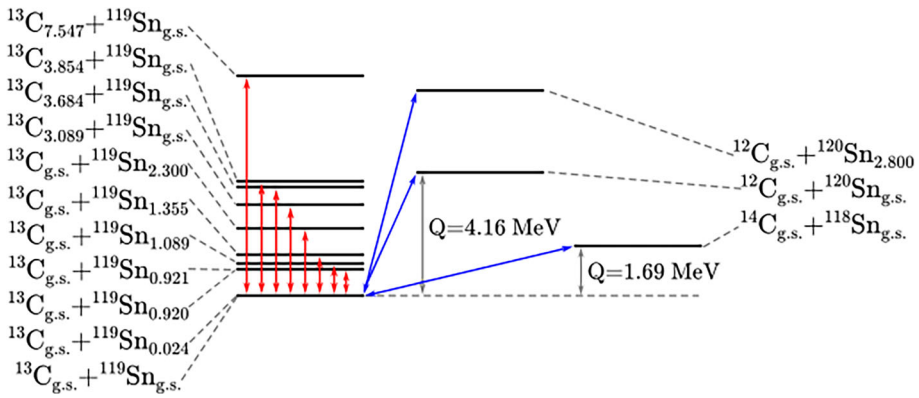

Fig. 3 Coupling scheme adopted in the CRC calculations. The red arrows indicate the inelastic couplings included in the initial mass partition, whereas the blue arrows correspond to the one neutron transfer couplings

Table 1 Spin, excitation energy (E^*, in MeV), transition multipolarity λ, transition strength from the ground-state (g.s.) to the excited states $B(E\lambda)\uparrow$ (in 10^{-3} e^2b^λ), and deformation length δ_λ (in fm) for the inelastic states included in the CRC calculations

Nucl	Spin	E^*	λ	$B(E\lambda)\uparrow$	δ_λ	References
^{13}C	$\frac{1}{2}^+$	3.09	1	0.14	0.083	[17]
^{13}C	$\frac{3}{2}^-$	3.68	2	1.37	1.66	[18]
^{13}C	$\frac{5}{2}^+$	3.85	3	0.22	1.42	[18]
^{13}C	$\frac{5}{2}^-$	7.55	2	2.05	1.42	[18]
^{119}Sn	$\frac{3}{2}^+$	0.0239	2	4.87	0.14	[19]
^{119}Sn	$\frac{3}{2}^+$	0.920	2	125	0.70	[9]
^{119}Sn	$\frac{5}{2}^+$	0.921	2	83.4	0.57	[9]
^{119}Sn	$\frac{5}{2}^+$	1.09	2	42.8	0.41	[9]
^{119}Sn	$\frac{5}{2}^+$	1.36	2	27.1	0.32	[9]
^{119}Sn	$\frac{5}{2}^+$	2.30	2	365	1.19	[9]

nearby levels are expected to have a negligible impact on the calculated elastic and inelastic observables at these energies.

Events associated with excited states of the projectile ($E^* > 3$ MeV) cannot be experimentally separated from those corresponding to transfer or excitation of the target. Additionally, yields from the target states at E^* around 2.30 MeV, reported in Ref.[9], could not be extracted from the spectra. Even so, they were included in the CRC calculations, as indicated in Table 1.

Single-nucleon transfer reactions represent a powerful tool in nuclear spectroscopy, providing valuable information about the structure of nuclei, such as single-particle energies, angular momentum assignments, and spectroscopic factors. They also play a crucial role in constraining theoretical models of reaction dynamics, offering insights into the interplay between nuclear structure and reaction mechanisms. Understanding these dynamics is essential for accurate modeling of more complex processes such as fusion, breakup, and multi-nucleon transfer, particularly in systems involving weakly bound or exotic nuclei.

In the present work, cross sections associated to the one-neutron stripping reaction, ^{119}Sn(^{13}C,^{12}C)^{120}Sn, were obtained for the ground-state (g.s.) and from the yields of a group containing a large number of excited states of the residual ^{120}Sn nucleus, spanning the excitation energy range $2.4 \leq E^* \leq 3.2$ MeV. For simplicity, CRC calculations were performed by assuming a single representative state at $E^* = 2.8$ MeV, with spin and parity $J = 5^-$, for this group of nearby populated states in the ^{120}Sn nucleus. The corresponding spectroscopic factor was adjusted to reproduce the magnitude of the transfer cross sections. This procedure is important to assess the influence of coupling unresolved states on the overall reaction dynamics.

For the one-neutron pickup reaction, ^{119}Sn(^{13}C,^{14}C)^{118}Sn, only the g.s. cross sections of the projectile and target overlaps were experimentally determined. However, as shown in Fig. 1, yields associated with other states at higher excitation energies are also visible in the spectrum. Nevertheless, extracting the corresponding cross sections is not straightforward, as the yields are significantly mixed due to the energy resolution of the detectors. Despite this limitation, estimates of the corresponding experimental cross sections were obtained.

In general, the effect of coupling the one-neutron pickup and stripping transfer channels on the measured elastic scattering angular distributions was found to be negligible, regardless of the chosen spin and spectroscopic factor values. It should be noted, however, that excited states of the ^{13}C and ^{119}Sn nuclei were not directly coupled to the transfer channels in the CRC calculations. While the influence of these channels is expected to be small for the elastic scattering observables, their omission could, in principle, affect the calculated transfer cross sections reported in this work [20,21].

Table 2 presents the particle-core spectroscopic factors ($C^2S_{\ell j}$) values for all projectile and target overlaps included in the CRC scheme. The $C^2S_{\ell j}$ value for the target overlap $\langle\, ^{120}\text{Sn} \mid\, ^{119}\text{Sn} + n \,\rangle$ corresponding to the excitation energy of 2.8 MeV was adjusted to reproduce the experimental data.

Table 2 Particle-core spectroscopic factors, $C^2S_{\ell j}$, for all projectile and target overlaps included in the CRC scheme. The parameter values of the WS potentials assumed for the cluster-core systems are also presented in the table

Overlap	E^* (MeV)	State $(n\ell j)$	$C^2S_{\ell j}$	V_0 (MeV)	R_0 (fm)	a (fm)
$\langle^{13}\mathrm{C} \mid {}^{12}\mathrm{C}+\mathrm{n}\rangle$	0.0	$1p_{1/2}$	0.76	50.8	2.40	0.81
$\langle^{120}\mathrm{Sn} \mid {}^{119}\mathrm{Sn}+\mathrm{n}\rangle$	0.0	$3s_{1/2}$	1.4	54.3	5.70	0.89
$\langle^{120}\mathrm{Sn} \mid {}^{119}\mathrm{Sn}+\mathrm{n}\rangle$	2.8	$1h_{11/2}$	3.6	49.6	5.70	0.89
$\langle^{14}\mathrm{C} \mid {}^{13}\mathrm{C}+\mathrm{n}\rangle$	0.0	$1p_{1/2}$	1.6	55.5	2.50	0.80
$\langle^{119}\mathrm{Sn} \mid {}^{118}\mathrm{Sn}+\mathrm{n}\rangle$	0.0	$3s_{1/2}$	0.42	49.6	5.70	0.89

The remaining spectroscopic factors used in the calculations, corresponding to the ground state of the nuclei, were taken from the literature [22,23]. The parameters of the WS shape assumed for the corresponding particle-core potentials are also listed in Table 2. The depths of the WS potentials were adjusted using the FRESCO code to reproduce the experimental separation energies corresponding to each partition. The geometry of the WS particle-core potentials was based on the shapes obtained from the SPP results.

3.2.1 *Elastic scattering*

Figure 4, displayed in (a) logarithmic and (b) linear scales, illustrates the effect of channel couplings on the elastic scattering angular distribution measured at 46.9 MeV. The solid red line corresponds to CRC calculations performed with the internal WS imaginary potential, whereas the dashed black line was obtained assuming $W(R) = 0.10\, V_{\mathrm{SPP}}(R)$.

Compared to the OM theoretical results (see panel (b) of Fig. 2), the CRC calculations significantly improve the overall agreement with the experimental data. In particular, adopting $W(R) = N_i\, V_{\mathrm{SPP}}(R)$ leads to better consistency with the elastic scattering data around the Coulomb-nuclear interference region, as the resulting CRC cross sections are attenuated relative to those obtained with the internal WS form. Notably, the normalization factor N_i required to reproduce the data within the CRC framework is three times smaller than that used in the OM analysis. This result underscores the role of channel couplings in the reaction dynamics and highlights the strong correlation between the imaginary potential strength and the inclusion of explicit coupling effects.

In this work, CRC calculations were also performed for the lower incident energy, $E_{\mathrm{Lab}} = 40.0$ MeV. As shown in Fig. 5, the inclusion of channel couplings improves the agreement with the experimental data compared to OM calculations, particularly when the imaginary part of the potential is modeled using an internal WS form. When the imaginary potential is instead defined as $W(R) = N_i\, V_{\mathrm{SPP}}(R)$, the data can be reproduced with significantly reduced absorption.

In addition, a noticeable suppression of the elastic cross section relative to the Rutherford prediction is observed

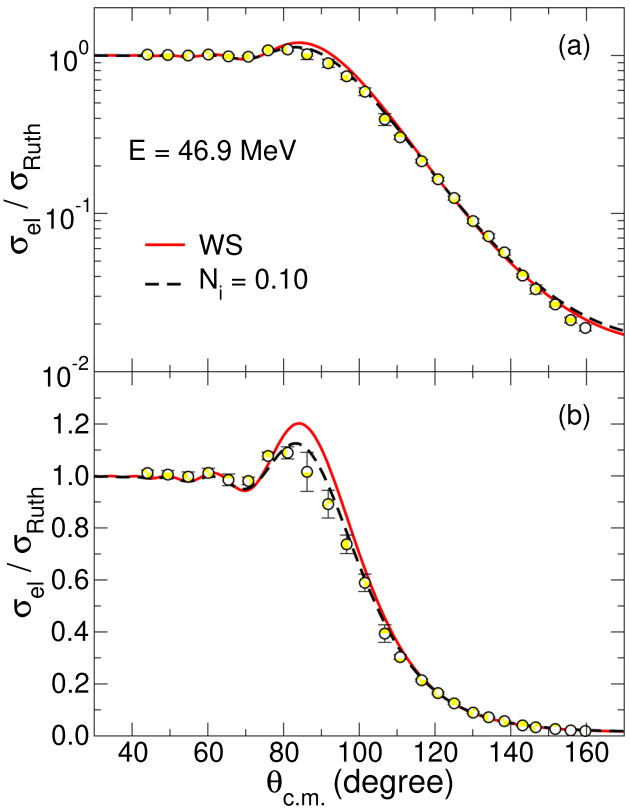

Fig. 4 Experimental cross sections for the elastic scattering of $^{13}\mathrm{C}+^{119}\mathrm{Sn}$ measured at 46.9 MeV bombarding energy, in **a** logarithmic and **b** linear scales. The solid red and dashed black lines are the CRC results obtained with an internal WS imaginary potential and assuming $W(R) = 0.10\, V_{\mathrm{SPP}}(R)$

at forward angles, as seen in Fig. 5. This feature, consistent with previous studies (e.g., [24–26]), reflects the dominance of long-range Coulomb excitation at low bombarding energies. In this angular region, where nuclear interactions are relatively weak, the depletion of elastic flux is primarily attributed to Coulomb excitation of low-lying collective states. To illustrate this effect, the dash-dotted green line in Fig. 5 shows CRC calculations including only the Coulomb interaction. In these calculations, the nuclear part of the interaction was switched off, so that the channel couplings arise exclusively from the Coulomb field.

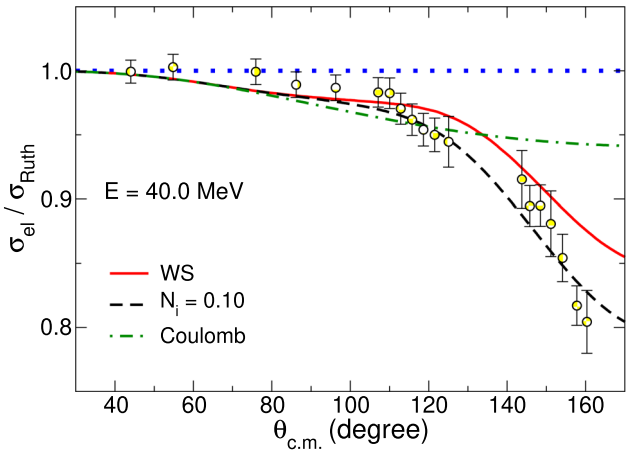

Fig. 5 Same as Fig. 4, but for $E_{\mathrm{Lab}} = 40.0$ MeV. The dotted blue line is drawn to guide the eyes

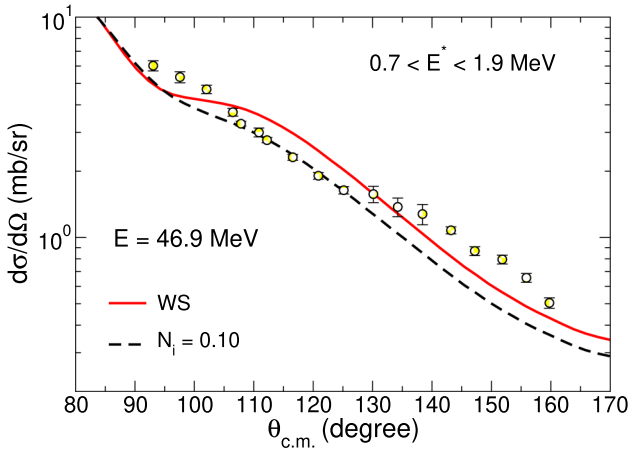

Fig. 6 Angular distribution of inelastic scattering cross sections for ^{119}Sn. The data correspond to the combined contribution of states with excitation energies in the range $0.7 \leq E^* \leq 1.9$ MeV. The lines represent CRC calculations (see text for details)

3.2.2 Inelastic scattering and transfer

Figure 6 presents the angular distribution of inelastic scattering cross sections associated with the excitation of states in the ^{119}Sn target. Due to limited energy resolution, individual contributions from states in the excitation energy range $0.7 \leq E^* \leq 1.9$ MeV could not be resolved in the spectra. Consequently, the experimental data correspond to the sum of cross sections for the ^{119}Sn states at $E^* = 0.920$, 0.921, 1.09, and 1.36 MeV. The solid red and dashed black lines in Fig. 6 represent the summed theoretical contributions from these states, obtained from CRC calculations assuming an internal WS imaginary potential and, respectively, a scaled SPP form with $N_i = 0.10$. The experimental data and theoretical predictions are in reasonable agreement. Although the theoretical curves do not fully reproduce the magnitude of the measured cross sections, their overall shape satisfactorily follows the observed trend, indicating a consistent description of the underlying reaction mechanism.

As previously mentioned, cross sections associated with one-neutron pickup and stripping reactions have been determined in the present work. Fig. 7 shows the experimental and theoretical cross sections for the population of the g.s. of both ^{14}C and ^{118}Sn. The results corresponding to the formation of the ^{12}C and ^{120}Sn residual nuclei in their g.s. (panel (a)) and in the excitation energies around 2.8 MeV (panel (b)) are presented in Fig. 8.

Overall, the CRC calculations provide a good description of the measured transfer cross sections. However, the coupling to transfer channels has a negligible impact on both the elastic and inelastic scattering angular distributions at both bombarding energies. This result is consistent with the findings reported in Ref. [9].

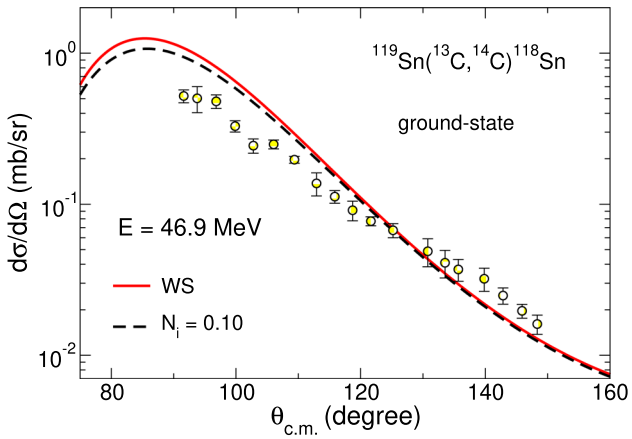

Fig. 7 Experimental cross sections for the one-neutron pickup transfer channel. The lines represent CRC calculations (see text for details)

3.2.3 Comparison of the ^{12,13}C +^{119} Sn elastic channel

An elastic scattering angular distribution for the ^{12}C+^{119}Sn reaction was recently published in Ref. [9]. Since that measurement was performed at the same bombarding energy as the present ^{13}C+^{119}Sn data, a direct comparison is instructive. Fig. 9 shows the angular distributions for both systems. Significant differences are observed around the rainbow region near 80°. Similar behavior has been observed, for instance, in the case of ^{20}Ne + ^{208}Pb compared to ^{22}Ne+^{208}Pb [27], where this effect was associated to differences in the inelastic couplings to the corresponding 2_1^+ excited projectiles states. Figure 9 also shows differences between the ^{12}C and ^{13}C elastic scattering angular distributions at larger angles ($\theta_{\mathrm{c.m.}} > 130°$). This suggests that, at this energy, the addition of one neutron to the projectile enhances the

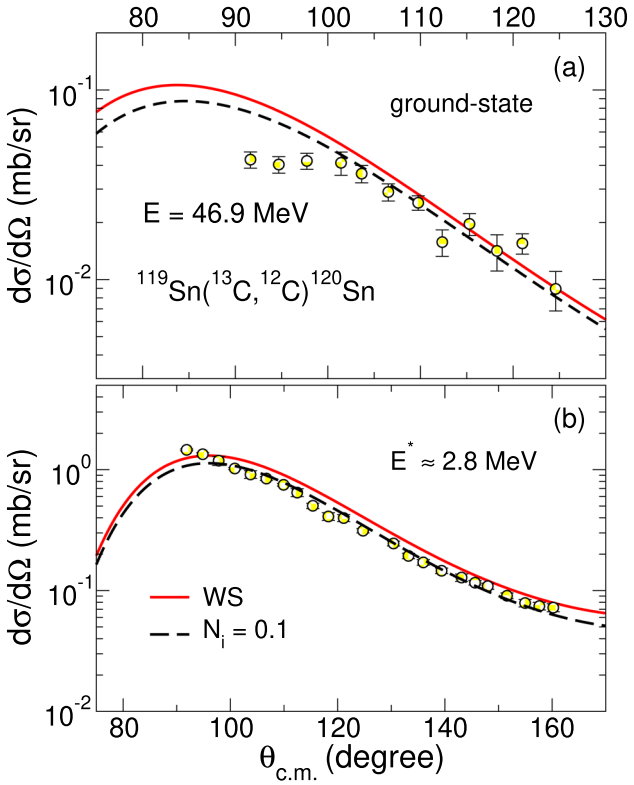

Fig. 8 Same as Fig. 7, but for the one-neutron stripping channel

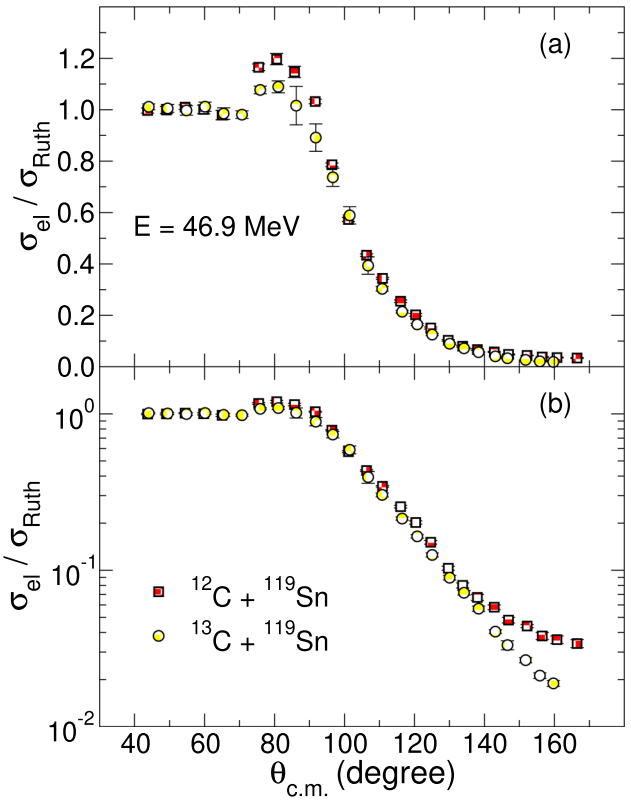

Fig. 9 Experimental cross sections for the elastic scattering of ^{12}C+^{119}Sn and ^{13}C+^{119}Sn at $E_{\mathrm{Lab}} = 46.9$ MeV

absorption of flux from the elastic channel into non-elastic processes.

4 Discussion and summary

In this work, new experimental data for the ^{13}C+^{119}Sn system were presented, including elastic scattering angular distributions at $E_{\mathrm{Lab}} = 40.0$ and 46.9 MeV, as well as inelastic and one-neutron transfer cross sections at 46.9 MeV. Optical model analyses using the São Paulo potential demonstrated that surface absorption is essential to describe the elastic data, particularly at intermediate angles, and that a purely internal imaginary potential fails to account for the observed features.

Coupled-reaction-channels calculations yielded an overall satisfactory description of the full data set. The inclusion of couplings to inelastic states significantly improved the agreement with the elastic-scattering data, while transfer couplings had only a negligible effect on both the elastic and inelastic angular distributions. The effect of including the spin–orbit potential for either the projectile or the target was also examined. At the bombarding energies considered in the present work, no systematic effect could be identified within the experimental uncertainties, and their impact on the elastic-scattering angular distributions is therefore negligible.

A comparison between the present results for ^{13}C+^{119}Sn and previous data for ^{12}C+^{119}Sn revealed significant differences, indicating that the presence of the additional valence neutron in ^{13}C modifies the reaction dynamics and leads to enhanced absorption through the combined effect of non-elastic channels, rather than through transfer alone.

These findings reinforce the importance of including detailed nuclear structure and coupling effects in reaction models.

Acknowledgements This work has been partially supported by Coordenação de Aperfeiçoamento de Pessoal de Nível Superior (CAPES) Proc. No 88887.834953/2023-00, Fundação de Amparo à Pesquisa do Estado de São Paulo (FAPESP) Proc. No 2024/23124-1, 2019/07767-1, 2021/11425-9, 2022/09060-5, 2024/01416-0, Conselho Nacional de Desenvolvimento Científico e Tecnológico (CNPq) Proc. No 302544/2022-4, 302072/2022-5, 315864/2023-0, and project INCT-FNA Proc. No 464898/2014-5. This work has also been partially supported by the Spanish Ministerio de Economía y Competitividad and FEDER funds (PGC2018-096994-B-C21), and by the project PAIDI 2020 with reference P20 01247, funded by the Consejería de Economía, Conocimiento, Empresas y Universidad, Junta de Andalucía (Spain) and by "ERDF A way of making Europe". This work is part of the project supported by the Spanish Ministerio de Ciencia, Innovación y Universidades (PID2023-146401NB-I00). This work has been partially supported by Ministerio de Universidades, project REC-B-22289-1. This work has been developed within the context of the IReNA (International Research Network for Nuclear Astrophysics) and the IANNA (Ibero-American Network of Nuclear Astrophysics). The authors acknowledge

all support and collaboration from IReNA and IANNA (National Science Foundation under Grant No. OISE-1927130).

Funding The Article Processing Charge (APC) for the publication of this research was funded by the Coordenação de Aperfeiçoamento de Pessoal de Nível Superior - Brasil (CAPES) (ROR identifier: 00x0ma614).

Data availability statement Data will be made available on reasonable request. [Author's comment: The datasets generated during and/or analysed during the current study are available from the corresponding author on reasonable request.].

Code availability statement This manuscript has no associated code/software. [Author's comment: Code/Software sharing not applicable to this article as no code/software was generated or analysed during the current study.].

References

1. D. Ridikas, M.H. Smedberg, J.S. Vaagen, M.V. Zhukov, Nucl. Phys. A **628**, 363 (1998)
2. N. Keeley, N. Alamanos, N. Single, Phys. Rep. **75**, 054610 (2007)
3. C.H. Rong, G.L. Zhang, L. Gan, Z.H. Li, L.C. Brandão, E.N. Cardozo, M.R. Cortes, Y.J. Li, J. Su, S.Q. Yan, S. Zeng, G. Lian, B. Guo, Y.B. Wang, W.P. Liu, J. Lubian, Chin. Phys. C **44**, 104003 (2020)
4. R. Linares, C.C. Seabra, V.A.B. Zagatto, V. Scarduelli, L. Gasques, L.C. Chamon, B.R. Gonçalves, D.R.M. Junior, A. Lépine-Szily, Phys. Rev. C **101**, 014611 (2020)
5. G. Yang et al., Chin. Phys. C **48**, 034001 (2024)
6. B.R. Gonçalves, D.R.M. Junior, R. Linares, V.A.B. Zagatto, C.C. Seabra, L.R. Gasques, V. Scarduelli, J.C. Zamora, L.C. Chamon, A. Lépine-Szily, Phys. Rev. C **109**, 044608 (2024)
7. R. Dubey, Atoms **13**, 33 (2025)
8. S.Y. Mezhevych, O.A. Ponkratenko, Y.M. Stepanenko, V.V. Uleshchenko, A. Rudchik, V.M. Kyrianchuk, Y.O. Shyrma, Y.S. Roznyuk, I.I. Vertegel, Nucl. Phys. Atom. Energy **26**, 31 (2025)
9. L.M. Martinis, L.R. Gasques, J.P. Fernández-García, V. Scarduelli, M.A.G. Alvarez, L.C. Chamon, W.A.Y. Hatano, J.K.L. Chaves, G.P. Cessel, L. Garrido-Gómez, Phys. Rev. C **111**, 034615 (2025)
10. L.C. Chamon et al., Phys. Rev. C **66**, 014610 (2002)
11. L.R. Gasques, Braz. J. Phys. **51**, 269 (2021)
12. D. Dell'Aquila, I. Lombardo, G. Verde, M. Vigilante, G. Ausanio, A. Ordine, M. Miranda, M.D. Luca, R. Alba, L. Augey, S. Barlini, E. Bonnet, B. Borderie et al., Nucl. Instrum. Methods A **877**, 227 (2018)
13. W. Milner, (UPAK Notes, Oak Ridge National Laboratory, 1994)
14. I.J. Thompson, Comp. Phys. Rep. **7**, 167 (1988)
15. D.F.M. Botero, L.C. Chamon, B.V. Carlson, J. Phys. G **44**, 105102 (2017)
16. L.C. Chamon, B.V. Carlson, Nucl. Phys. A **846**, 1 (2010)
17. E.K. Warburton, D.E. Alburger, D.J. Millener, Phys. Rev. C **22**, 2330 (1980)
18. S.A. Goncharov, A.S. Demyanova, A.N. Danilov, V.I. Starastsin, T.L. Belyaeva, W. Trzaska, N. Burtebayev, M. Nasurlla, Y.B. Gurov, Phys. Atom. Nuclei **85**, 785 (2022)
19. D.M. Symochko, E. Browne, J.K. Tuli, Nucl. Data Sheets **110**, 2945 (2009)
20. A. Spatafora, D. Carbone, F. Cappuzzello, M. Cavallaro, L. Acosta, C. Agodi, P. Amador-Valenzuela, T. Borello-Lewin, G.A. Brischetto, S. Calabrese, D. Calvo, V. Capirossi, E.R.C. Lomelí, I. Ciraldo, G.D. Gregorio, F. Delaunay, H. Djapo, C. Eke, P. Finocchiaro, S. Firat, M. Fisichella, A. Foti, A. Gargano, A. Hacisalihoglu, F. Iazzi, L.L. Fauci, R. Linares, J. Lubian, N. Medina, M. Moralles, J.R.B. Oliveira, A. Pakou, L. Pandola, H. Petrascu, F. Pinna, G. Russo, O. Sgouros, M.A.G. da Silveira, S.O. Solakci, V. Soukeras, G. Souliotis, D. Torresi, S. Tudisco, A. Yildirim, V.A.B. Zagatto, Phys. Rev. C **107**, 024605 (2023)
21. R. Linares, C.C. Seabra, V.A.B. Zagatto, F. Cappuzzello, M. Cavallaro, D. Carbone, C. Agodi, L.M. Fonseca, J.R.B. Oliveira, Phys. Rev. C **108**, 014619 (2023)
22. J. Lee, M.B. Tsang, W.G. Lynch, Phys. Rev. C **75**, 064320 (2007)
23. L. Gan et al., Phys. Rev. C **101**, 014612 (2020)
24. N. Keeley, K.W. Kemper, K. Rusek, Eur. Phys. J. A **50**, 145 (2014)
25. L.C. Chamon, D. Pereira, E.S. Rossi Jr., C.P. Silva, R. Lichtenthäler, L.C. Gomes, Nucl. Phys. A **582**, 305 (1995)
26. L.C. Chamon, D. Pereira, E.S. Rossi Jr., C.P. Silva, H. Dias, L. Losano, C.A.P. Ceneviva, Nucl. Phys. A **597**, 253 (1996)
27. E.E. Gross, T.P. Cleary, J.L.C. Ford Jr., D.C. Hensley, K.S. Toth, F.T. Baker, A. Scott, C.R. Bingham, J.A. Vrba, Phys. Rev. C **29**, 459 (1984)